

Spaceborne GNSS-Receiving System Performance Prediction and Validation

M. Sust⁽¹⁾, F. Zangerl⁽¹⁾, O. Montenbruck⁽²⁾, S. Buchert⁽³⁾, A. Garcia-Rodriguez⁽⁴⁾

⁽¹⁾ *RUAG Space GmbH*

Stachegasse 13, 1120 Vienna, Austria

Email: manfred.sust@ruag.com, franz.zangerl@ruag.com

⁽²⁾ *Deutsches Zentrum für Luft- und Raumfahrt (DLR)*

Oberpfaffenhofen, 82234 Wessling, Germany

Email: oliver.montenbruck@dlr.de

⁽³⁾ *Swedish Institute of Space Physics (IRF)*

Box 537, SE-751 21 Uppsala, Sweden

Email: scb@irfu.se

⁽⁴⁾ *European Space Research and Technology Centre (ESTEC)*

Keplerlaan 1, 2201 AZ Noordwijk, Netherlands

Email: alberto.garcia@esa.int

INTRODUCTION

Spaceborne high-end geodetic-type dual-frequency Global Navigation Satellite System (GNSS) receivers have become an enabling technology for contemporary earth observation missions in Low-Earth Orbits (LEO). Such receivers deliver measurements for space vehicle Precise Orbit Determination (POD) with position accuracy of a few centimeters to geolocate the measurements taken by other sensors. Roughly speaking, the more precise an earth-observation instrument, the more accurate its position must be determined in order to be able to produce accurate measurement maps. In addition, real-time positioning, accurate within meters - a byproduct of POD-receivers - performed for internal purposes, readily supports the Attitude and Orbit Control Subsystem (AOCS) of the host Spacecraft (S/C).

While the notion of recurrence and off-the-shelf availability is reflected in customer price and delivery schedule expectations, POD-receivers are typically procured according to mission specifications concerning performance under a broad range of boundary conditions. This is due to the fact that knowledge concerning important issues like antenna accommodation, maneuvers and on-board interference environment only gradually evolve during the course of the mission design and that the space environment is always good for a surprise. Consequently, accurate performance prediction techniques are of paramount importance to avoid disappointment on the one hand and over-specification on the other.

In the present paper we place emphasis on the verification component of our spaceborne GNSS-Receiver (GNSSR) product platform which we routinely apply for product end-to-end testing, design validation and systems engineering purposes. The latter goes far beyond the level of usual feasibility studies in that in-orbit measurement data can be analyzed and fed back into the design process for optimizing both receivers and verification platform.

After a brief introduction of our spaceborne GNSS-receivers and the ground test- and system-in-the loop simulation environment, we present results of the evaluation of initial in-orbit measurements provided by the three SWARM GPS receivers during the commissioning phase which widely overlapped with a period of increased solar activity, resembling a stress case for a high precision dual-frequency POD receiver. Our analyses concern carrier-, code-phase, signal-to-noise ratio, real-time positioning as well as POD and show that the receivers work very well within their specifications due to considerate design margins but they also reveal subtle differences between real space conditions and models typically used for system simulation and GNSS satellite simulator based ground testing.

SPACEBORNE GNSS-RECEIVER PLATFORM

The embedded spaceborne GNSS-receiver platform from which particular product offerings can be derived consists of a hardware- and a software component. As illustrated by the examples provided in Fig. 1, the hardware platform resembles a standard receiver architecture consisting of several types of antennas, Low-Noise Amplifiers (LNAs), power converters and spacecraft interfaces, a configurable Radio-Frequency (RF) front-end module and two types of digital processing modules, containing analog-to-digital conversion, digital signal processing, as well as a programmable processor. The latter hosts the receiver software, responsible for signal acquisition and tracking and for retrieving raw measurements, referred to as measurement processing, for computing a navigation solution, performing receiver control and for handling the interface to the S/C-computer. In Fig. 2 the receiver software platform elements are shown in their hardware context.

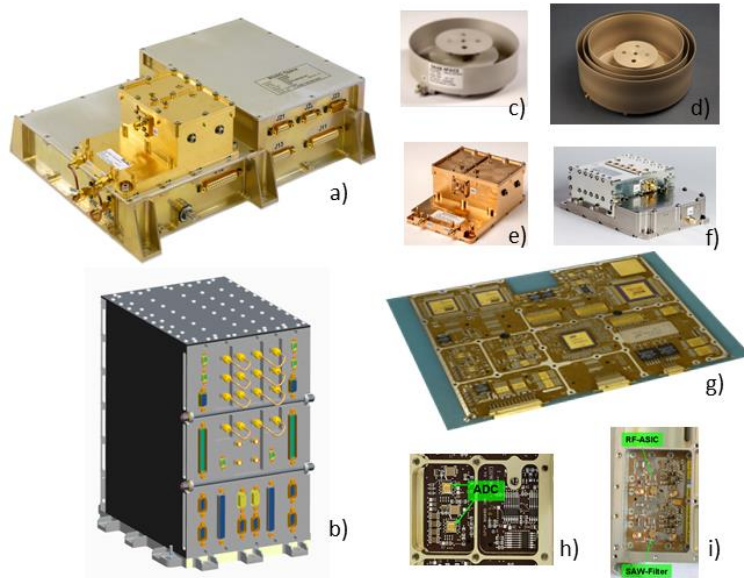


Fig. 1 - Examples of POD-receiver hardware platform elements: a) Stand-alone receiver mechanics, b) Plug-in receiver mechanics alternative, c) Low-multipath POD antenna, d) Very-low multipath POD antenna, e) Dual-Frequency LNA, f) Triple Frequency LNA, g) Channel- and navigation processing electronics core, h) ADC-module, i) RF-module

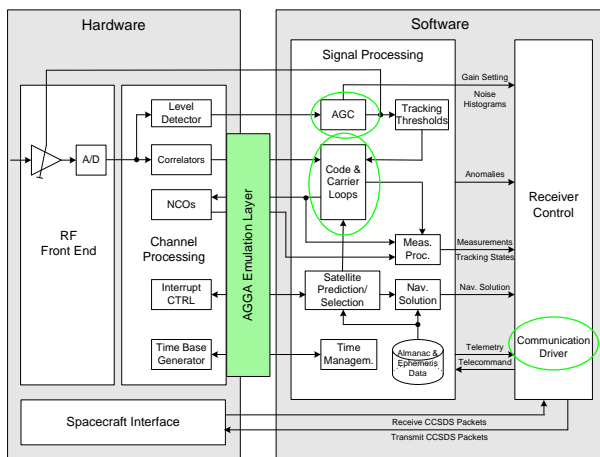


Fig. 2 - Embedded receiver software platform elements

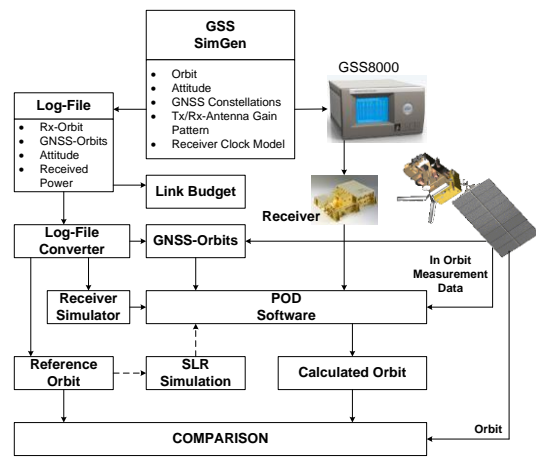


Fig. 3 - System simulation environment

The receiver platform elements are shared between the current generation of RUAG POD receiving systems, referred to as GPSR-G2, and the next generation of so called SpacePOD receivers, which have been kept as compatible to their predecessors as possible [1]. GPSR-G2 offers dual-frequency capability based on the GPS L1-C/A, L2-P(Y) and L2C signals. SpacePOD is able to process GPS-L5 in addition to L1-C/A, L2-P(Y) and L2C as well as GALILEO E1 and E5a, GLONASS-CDMA and BeiDou signals. Consequently, the greatest differences between the receiver generations concern the digital processing modules which are exclusively based on the AGGA-2 channel processing Application Specific Integrated Circuit (ASIC) for GPRS-G2, while for SpacePOD the AGGA-4 [2] is employed as processing core. Both ASICs, developed by the European Space Agency (ESA), have a common root and the same basic architecture as far as GNSS signal processing is concerned. Since RUAG Space was involved in both ASIC developments, in particular in their validation and interface definition, the receiver software platform, which has evolved over a period of almost 15 years, has been using a standardized AGGA emulation layer from the very beginning. Further, the programmable processor, viz. a LEON-2-FT, has remained. Consequently, as a first step, legacy software platform elements were fully re-used to accomplish legacy functionality with the next receiver generation. Full SpacePOD functionality, exploiting the AGGA-4 to its full extent, was achieved by additional software modules in support of new signals and features. Regression testing, well supported by the verification platform described below, has ensured lossless transfer of GPSR-G2 heritage to SpacePOD. This development approach facilitates temporary co-existence of both generations, minimizes customer risk and maximizes continuity.

observation instruments providing inputs to ground algorithms for sub-decimeter-level POD and for the determination of the Total Electron Content (TEC) along the GPS-signal path. Therefore, the accuracy of the carrier and code phase measurements is of primary concern.

On-Ground Verification

The SWARM on-ground verification approach aimed at demonstrating that all key performance parameters were met for realistic scenarios even under pessimistic assumptions concerning the GPS constellation. The tests were performed using the test environment of Fig. 4, albeit with a Spirent 4760 as stimuli equipment. The user trajectories simulated parts of the actual SWARM orbit, including orbit correction and attitude maneuvers. Signal levels were very pessimistically adjusted according to a worst case link budget based on guaranteed GPS signal power levels and the receiver antenna gain pattern specification.

Since measurement errors common for all measurements are mapped into negligibly small time errors by real-time navigation or POD processing, on-ground testing zoomed on individual error contributions due to thermal noise and local multipath, respectively. Thermal noise induced errors were determined by means of a double-difference zero baseline test. Apart from antenna accommodation simulations the antenna gain- and phase patterns were measured with the antenna mounted on a spacecraft mock-up to verify the performance in the actual spacecraft environment [5]. Table 1 allows for comparing multipath and random noise errors, revealing that for the carrier phases, which are most relevant for POD performance, the former is dominant. For the determination of the total error the two error contributions can be assumed to be independent.

Table 1 - Code and carrier phase performance at 0.1 Hz sample rate (L2 with anti-spoofing (AS) on).

Parameter	Carrier L1/L2 [mm]	Code CA/ P(Y) [m]
Thermal noise standard deviation over 15° - 90°	0.8/2.9	0.13/0.27
Estimated multipath bias	2.5/4	0.1/0.16
Total rms accuracy	3.0/5.0	0.16/0.31

GPS-satellite simulator based system tests based on realistic SWARM scenarii were used throughout the ground test campaign including space-environmental testing (thermal vacuum and vibration). Apart from exercising various interference threats, atmospheric propagation was modelled using capabilities and models readily provided by the satellite simulator [6]. Due to limited knowledge about the fine structure of the Ionosphere to be expected along the GPS-SWARM ray-path, only smooth ionosphere models were employed for testing the dual-frequency receiver's ionospheric delay resolution capabilities.

In-Orbit Validation

After the successful launch of the SWARM satellites end of November 2013, in-orbit validation of the GPS receivers during the commissioning phase aimed at proving full functionality and performance in spite of being exposed to launch stress and space environmental conditions. This phase was concluded successfully with the result that all assessed performances were as good as or even better than expected. In particular,

- the three receivers did not show any differences with respect to behavior or performance,
- all three receivers passed all functional checks successfully and
- the measured C/N_0 was up to 6 dB higher than had been assumed by the worst case links budget.

Nevertheless, evaluation of the carrier phase showed unexpected results, which can now with high probability be attributed to the fine structure of the Ionosphere at and near spacecraft altitudes.

Evidently, some of the evaluation methods applied during on-ground testing are not applicable for in-orbit validation due to the lack of true reference data. As carrier phase errors are smaller than code phase errors by orders of magnitude, code phase performance can be determined by de-trending the code phase with the locally estimated carrier phase. However, as the carrier phase is the main data product for POD, evaluation of the carrier phase performance is most crucial but inevitably requires removal of the geometric phase evolution caused by the movement of the receiver relative to the transmitter, which may in turn introduce disturbances to the data. Upon careful consideration and relying on the quality of the on-ground testing, a simple de-trending approach based on multiple differentiations was selected as baseline. This approach allows for qualitative rather than quantitative evaluation of the carrier phase, which was considered adequate when simply searching for potential receiver anomalies by comparing on-board performance with on-ground reference tests. Results of the latter are represented by the left plot of Fig. 5, showing the aligned de-trended carrier phases of several tracks sampled at a rate of 0.1 Hz. Clearly, the C/N_0 values along each track vary according to the link budget for the simulated LEO scenario. For comparison, the right plot depicts de-trended L1-carrier phase measurements made by the SWARM GPS receiver during one "work day" in orbit. Different colors distinguish the eight tracking channels associated with different GPS Space Vehicles (SVs). The on-ground pattern can be clearly spotted in these plots, even with lower variance due to unconsumed link-budget margins, but such "normal" or "good"

periods are interrupted by “bad” intervals with considerably higher disturbances. In addition, the receivers reported events never observed during on-ground testing such as cycle slips and even tracking loss of lock.

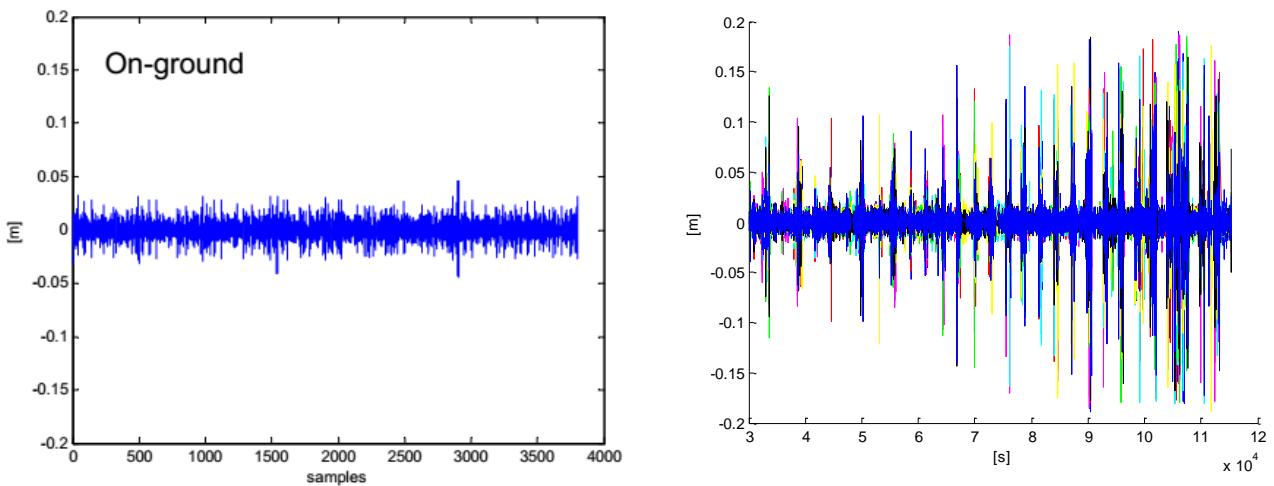


Fig. 5 – Comparison of de-trended L1 carrier phases measured on-ground (left, $T_s=10s$) and in-orbit (right)

Fig. 6 shows details of de-trended carrier phase records during a period of approximately 30 minutes, exhibiting excessive phase variations. Again color coding allows for distinguishing eight receiver channels which are all affected, however, fairly different with respect to timeliness and magnitude of the disturbances. The L2 behavior is similar to the one of L1 which may be partially attributed to the fact that the L2 loop is cross-aided by the L1 carrier tracking, but on the other hand the magnitude and in particular the timing is such that the greatest part of the correlation seems to be introduced by a strongly related or even identical effect with frequency dependent impact with respect to modulation strength and propagation delay.

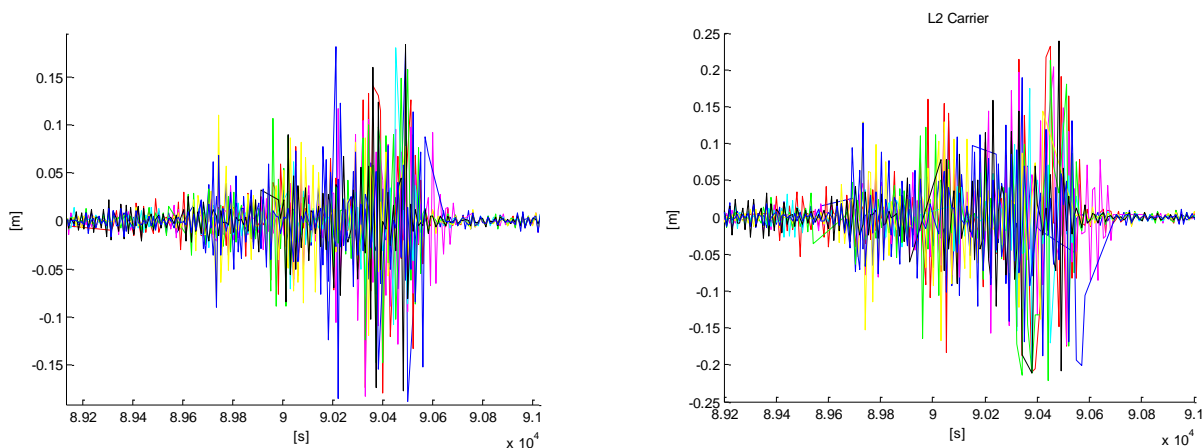


Fig. 6 - Zooms of de-trended L1 (left) and L2 (right) carrier phases

An assessment of the on-board carrier-to-noise ratio (C/N_0) estimates showed that phase disturbances were not at all associated with low C/N_0 levels, but fairly evenly distributed, that they occurred even at high C/N_0 values and that on the other hand high C/N_0 never violated the assumption of receiver linearity. Amplitude fades could not be observed at all.

The behavior of the three receivers hosted on SWARM A, B and C, flying in close vicinity, appeared to be highly correlated. Already at this point receiver-hardware degradation could be excluded as possible cause because the phase measurements were not always disturbed but the disturbances occurred in almost regular intervals. A hardware problem with stochastic appearance is very unlikely to affect the three different receivers simultaneously. Further, the effects on L1 and L2 would be uncorrelated as L1 and L2 are processed in separate analog signal paths. Down-conversion chain errors would affect the measurements of all receiver channels in the same way.

Similar considerations and conclusions apply to the investigation of single-event radiation effects, but in this case additional information is available in form of time tagged radiation event logs provided by the error-detection and

correction circuitry hosted on the GPSP-board. As predicted by radiation analyses, single-event effects have to be counteracted by the receiver fairly regularly, but radiation-log and carrier-phase data appear completely uncorrelated.

While low probability of unintentional on-board interference can be assumed due to the stringent Electromagnetic Compatibility (EMC) regime exercised during the spacecraft development, spaceborne receivers have been reported to be affected by terrestrial interference [7], albeit at the lower GNSS frequencies, in particular L5/E5 and L2, rather in the northern hemisphere and most frequently and most pronounced in the region near the north pole. On the other hand, we have not found any mentioning about interference near south pole regions.

Fig. 7 depicts noise power measurements of one receiver for a period of three orbits. While the L1 noise is very stable noise power disturbances and switching of the automatic gain control (AGC) can be observed on L2 during north-pole passes. Although there is no doubt that this behavior is due to interference which is also visible on code and carrier-phase observables, this only explains a vanishingly small part of disturbances and only for L2.

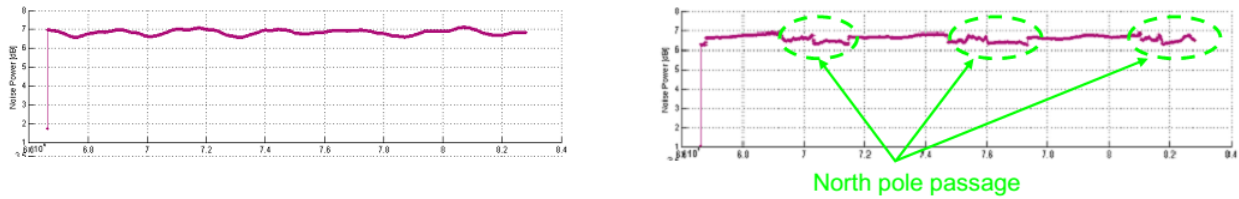


Fig. 7– Measured noise power on L1 (left) and L2 (right)

Ionospheric scintillations are known to be the cause for phase disturbances, cycle slips and loss of phase-tracking lock, but were initially not expected to be a severe problem for a receiver with a zenith pointing antenna at an altitude of almost 500 km. While there is increasing knowledge about scintillation effects experienced by ground receivers and empirical models for testing their scintillation robustness are improving, first-principles physics-based models providing sufficient information about geographical location, altitude, extent and properties of ionospheric irregularities such that geometrical mapping could be applied to obtain representative time series of the atmospheric modulation added to GNSS signals during signal propagation do not seem to be available [8]. From a receiver point of view it is reasonable to distinguish between amplitude and phase scintillations. For the SWARM receiver only the latter seem to be an issue. Roughly speaking, scintillation type, probability of occurrence and intensity depend at least on solar activity, geographic location, season and local time. For a spaceborne receiver also antenna orientation and spacecraft altitude are influential.

According to literature [9], scintillations are most pronounced in two bands of about ± 15 degrees around the magnetic equator and in regions around the magnetic poles. It is worthwhile to distinguish between diffractive scintillations caused by scattering in an irregular ionosphere, which lead to both amplitude and phase variations of the received signal, and refractive scintillations, pre-dominantly experienced as phase fluctuations. The strong equatorial scintillations are primarily of the first kind, their maximum occurs in the evening after sunset and intensity and timely behavior can be explained by irregularities developing under solar influence at altitudes between 300 and 400 km. Although this is below SWARM, the irregularities may form at any altitude and at higher altitudes refractive scintillations - for ground receivers probably masked by the strong diffractive scintillation components - may very well be an issue.

Polar ionospheric irregularities are associated with fairly low electron densities so that diffraction is not an issue. However, refractive scintillations in the form of the time rate of change of TEC were observed with TEC changing by 2 TECU per minute on the edges of polar cap patches with peak vertical TEC values of about 10 TECU. Such TEC variations can cause significant phase fluctuations of GPS signals. Reported phase fluctuations are largest in the auroral oval near magnetic midnight which is the time of day when an observer on earth, the North- or South- Magnetic Pole and the sun are aligned. Apparently, polar scintillations depend on magnetic and auroral activity and so far it was not possible to determine the irregularity height [10].

In Fig. 8 we aim at geo-locating unexpected receiver behavior in a magnetic field map, starting with the most severe events occurring end of January and beginning of February 2014, where in the evening hours of local time all three SWARM GPS receivers repeatedly reported that they had lost so many channels that a kinematic navigation solution could not be computed any longer and that only a dynamic solution could be provided. The loss of lock had occurred on several channels almost simultaneously and in most cases was preceded by tracking problems of L2. Note that for codeless tracking of the P(Y) signals the L2 carrier loop has a significantly smaller bandwidth than the L1 carrier tracking loop (1 Hz vs. 10 Hz). In any case C/N_0 was virtually constant and high enough for robust tracking.

Apart from the serious event of the number of tracked satellites falling below the level necessary for performing kinematic positioning, loss-of-lock for single tracking channels was in fact found to have occurred more frequently. In the observation period of about one month about 200 losses of the L1 signal were reported for each of the three receivers at the locations indicated in Fig. 9. Also here, the majority of the events occurred near the magnetic equator in the evening hours, only a few in polar regions and none at mid latitudes.

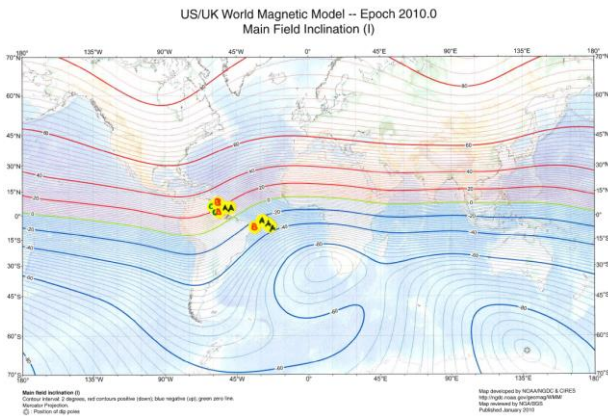


Fig. 8 - Geolocation of invalid navigation events

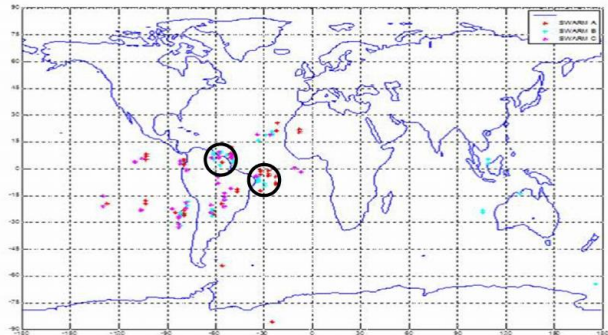


Fig. 9 - Geolocation of loss of lock events

A finer picture is obtained with Fig. 10, where carrier-phase disturbances similar to the examples shown in Fig. 5 and Fig. 6 are geo-located. Most of the events occur in equatorial and polar regions. It is noticeable that equatorial events occur exclusively in the evening, while the same region can be passed without problems in the morning.

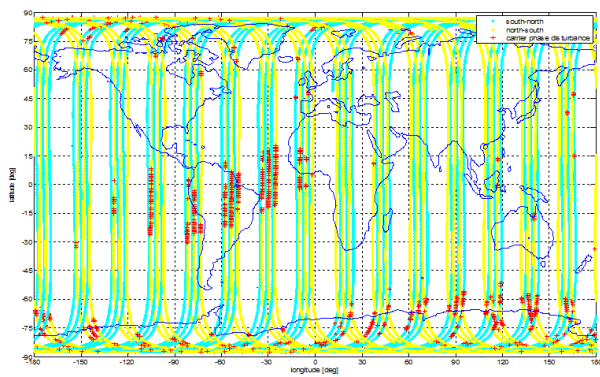


Fig. 10 - Geo-location of carrier-phase disturbances (yellow track: equator crossed in the evening, blue track: equator crossed in the morning)

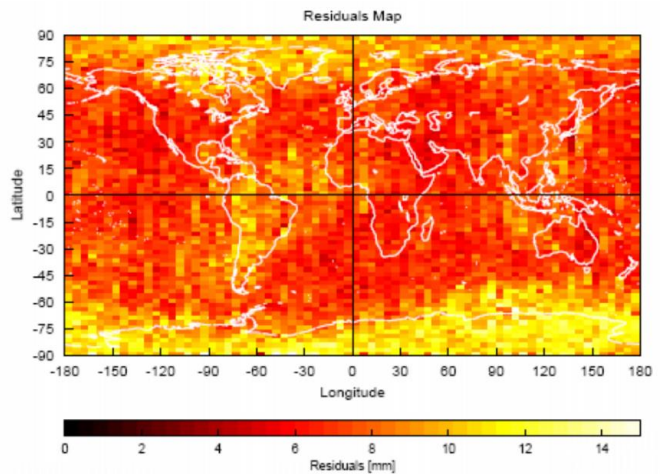


Fig. 11 - Carrier phase residual as a result of POD processing

Ultimate de-trending is most probably obtained by using POD to remove the geometric phase contribution, which is represented by Fig. 11 in form of POD phase residuals for the same observation period. Comparison with Fig. 10 shows excellent agreement but has to be done carefully, as both plots are based on some threshold values. While a disturbance threshold must be exceeded to be eligible for representation in Fig. 10 exceeding a certain threshold of the POD pre-processor may result in being discarded completely from the data set so that Fig. 11 expectedly emphasizes phase errors in the polar regions where phase variations are high, but below the validity threshold.

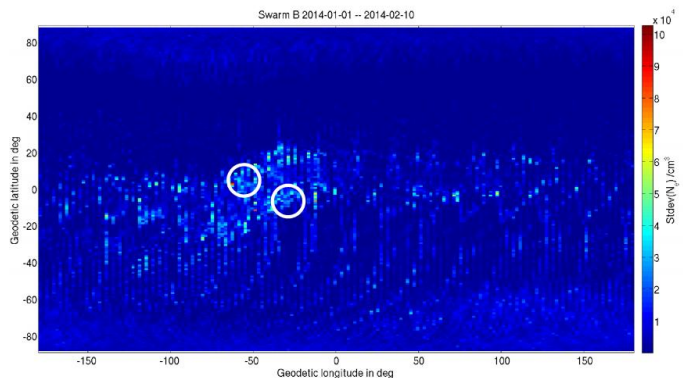


Fig. 12 - Map of electron density variations

Finally, the results of receiver-data evaluations compare well with the in-situ electron-density measurements taken during the same time period with the Langmuir

probes being part of the SWARM Electric Field Instrument (Fig. 12). The density variation is calculated from 15 s long slices (corresponding to 31 samples) of electron density measurements by the Langmuir probe. Each slice is detrended and the standard deviation of the residuals serves as indicator for the density variability. Receiver event zones coincide with areas of noticeable in-situ electron-density variations. The comparison does not only hold with respect to severe disturbances but also concerning the seasonal effect that the southern hemisphere is more affected than the northern part. Fig. 12 also shows noticeable variations in regions where this would not have been expected, thereby anticipating less expected phase disturbances in Fig. 10 and Fig. 11.

CONCLUSIONS

In-orbit validation of the SWARM GPS receivers during the spacecraft commissioning phase aiming at proving receiver functionality and performance after having been exposed to launch stress was successful with the result that the receiver did not only meet all specifications but that all assessed performances were as good as or even better than expected.

Within the frame of this campaign also the receiver manufacturer's tools for performance prediction, verification and qualification were validated and important conclusions for their further improvement could be drawn.

Beyond this scope, evaluation of the carrier phase has brought forth unexpected results, which we have been able to trace back to ionospheric scintillations. Although the SWARM GPS receiver development was supported by an elaborate verification concept, the used atmospheric propagation models could not predict ionospheric irregularities as encountered during the phase of increased solar and magnetic activity witnessed at the beginning of 2014. In addition to the fact that the orbits of the SWARM spacecraft are particularly suited for studying the influence the Ionosphere has on GNSS receiving systems, having had access to receiver data from this period is considered particular luck as with end of February 2014 the more severe events reported in this paper have ceased.

ACKNOWLEDGMENTS

The authors wish to thank numerous colleagues at RUAG Space GmbH for providing the basis for the present paper. Development of the described GNSS receiver platforms has been performed under various ESA contracts as well as with support from the Austrian Research Promotion Agency (FFG). In this context, valuable contributions by ESA staff and in particular by Nico Stricker and Gustavo Lopez are gratefully acknowledged. Thanks are also due to the members of the SWARM and SENTINEL project teams of Airbus Defence and Space and Thales-Alenia Space.

REFERENCES

- [1] M. Sust, A. Carlström, and A. Garcia-Rodriguez, "European Spaceborne Dual Frequency GPS Receiver for Science and Earth Observation," *Proceedings of the 22nd International Technical Meeting of the Satellite Division of the Institute of Navigation (ION GNSS)*, 2009, pp. 1419–1426.
- [2] J. Roselló, P. Silvestrin, G. L. Risueño, R. Weigand, J. V. Perelló, J. Heim, and I. Tejerina, "AGGA-4: Core Device for GNSS Space Receivers of this Decade," *Proceedings of the 5th ESA Workshop on Satellite Navigation Technologies (NAVITEC) and European Workshop on GNSS Signals and Signal Processing*, 2010.
- [3] ESA's Magnetic Field Mission SWARM, http://www.esa.int/Our_Activities/Observing_the_Earth/The_Living_Planet_Programme/Earth_Explorers/Swarm, accessed 20-Aug-2014.
- [4] O. Montenbruck, Y. Andres, H. Bock, T. Van Helleputte, J. Van Den IJssel, M. Loiselet, C. Marquardt, P. Silvestrin, P. Visser, and Y. Yoon, "Tracking and orbit determination performance of the GRAS instrument on MetOp-A," *GPS Solutions*, vol. 12, no. 4, pp. 289–299, 2008.
- [5] J. Wettergren, M. Bonnedal, P. Ingvarson, and B. Wästberg, "Antenna for precise orbit determination," *Acta Astronautica*, vol. 65, no. 11–12, pp. 1765–1771, Dec. 2009.
- [6] SIMGEN Software User Manual, Spirent, DGP00686AAA, Issue 4-03, 2013.
- [7] O. Isoz, S. A. Buehler, K. Kinch, M. Bonnedal, and D. M. Akos, "Interference from terrestrial sources and its impact on the GRAS GPS radio occultation receiver," *Radio Science*, vol. 49, no. 1, pp. 1–6, 2014.
- [8] T. E. Humphreys, M. L. Psiaki, J. C. Hinks, B. O'Hanlon, and P. M. Kintner, "Simulating ionosphere-induced scintillation for testing GPS receiver phase tracking loops," *IEEE Journal of Selected Topics in Signal Processing*, vol. 3, no. 4, pp. 707–715, 2009.
- [9] P. M. Kintner, T. E. Humphreys, and J. Hinks, "GNSS and ionospheric scintillation - How to Survive the Next Solar Maximum," *Inside GNSS*, vol. 4, no. 4, pp. 22–31, 2009.
- [10] P. M. Kintner, B. M. Ledvina, and E. R. de Paula, "GPS and ionospheric scintillations," *Space Weather*, vol. 5, no. 9, p. S09003, Sep. 2007.
- [11] F. S. Rodrigues, M. C. Kelley, P. A. Roddy, D. E. Hunton, R. F. Pfaff, O. de La Beaujardière, and G. S. Bust, "C/NOFS observations of intermediate and transitional scale-size equatorial spread F irregularities," *Geophysical Research Letters*, vol. 36, no. 18, 2009.